Received May 6, 2019, accepted May 29, 2019, date of publication June 3, 2019, date of current version June 19, 2019.

Digital Object Identifier 10.1109/ACCESS.2019.2920518

On the Development of a Simulation Strategy to Model the Behavior of Graphene-Based Devices in Electromagnetic Simulators

ANDREEA IOANNA HADARIG[1], SAMUEL VER HOEYE[1], (Member, IEEE), MIGUEL FERNÁNDEZ[1], SERGEY MIKHAILOV[2], CARLOS VÁZQUEZ[1], LETICIA ALONSO[1], (Student Member, IEEE), AND FERNANDO LAS-HERAS[1], (Senior Member, IEEE)

[1]Department of Electrical Engineering, University of Oviedo, E33203 Gijón, Spain
[2]Department of Physics, University of Augsburg, 86135 Augsburg, Germany

Corresponding author: Miguel Fernández (fernandezgmiguel@uniovi.es)

This work was supported in part by the European Union Seventh Framework Programme (FP/2007-2013) under Project 600849, in part by the Spanish Agencia Estatal de Investigación (AEI) and Fondo Europeo de Desarrollo Regional (FEDER) under Project TEC2016-80815-P (AEI/FEDER, UE) and Project TEC2015-72110-EXP (AEI), in part by the Gobierno del Principado de Asturias (PCTI) and FEDER under Project IDI/2016/000372, Project IDI/2017/000083, and Project IDI/2018/000191, and in part by the European Union Horizon 2020 Research and Innovation Programme Graphene Core 2 under Grant Agreement 785219.

ABSTRACT This paper presents a new simulation strategy to be implemented in electromagnetic simulators in order to calculate the level of the induced high-order harmonic components in mono- and bi-layer graphene flakes when they are driven by an input electromagnetic field and to evaluate the frequency response of structures, including graphene. The technique is applied to the design and analysis of a single-stage high-order frequency multiplier capable of generating an output signal in the 220–330-GHz range from an input signal in the 26–40-GHz bands, whose topology is based on a structured graphene sheet enclosed in a waveguide resonant cavity that maximizes the incident electromagnetic field. A prototype was implemented to validate the method, obtaining a good agreement with the simulation results. Furthermore, the prototype was also used to experimentally characterize the performance of the multi-layer graphene sheets. In this case, the developed model is used to calculate the frequency response of the structure, but it is not able to predict the output power since the mathematical model describing the frequency conversion phenomena cannot be extrapolated to the multi-layer graphene. Several configurations were tested in order to determine the influence of the graphene sheet's thickness and shape on the output power. Finally, a −33-dBm level output signal at 280 GHz was generated as the seventh-harmonic component of an input signal with a frequency of 40 GHz, showing that the presented prototype can be used as a signal generator in practical submillimeter-wave applications.

INDEX TERMS Circuit simulation, frequency multipliers, graphene, stereolithography, submillimeter wave circuits.

I. INTRODUCTION

In recent years, an overwhelming variety of applications in submillimeter and low THz frequency bands have been proposed in technical literature. The non-harmful nature of electromagnetic radiation in these frequency bands, its penetration properties, and the continuously increasing knowledge of the characteristic response exhibited by a wide variety of substances and biological entities, makes it very suitable for applications in fields as diverse as security [1], medicine [2]–[5], pharmaceuticals [6], imaging [7], [8], or nondestructive testing [9], among many others. Despite the expected great impact of the potential applications, the cost-effective implementation of signal generators and detectors represents a technological bottleneck which seriously limits their practical development.

Signal generation [10], [11] and detection [12], [13] in the submillimeter wave and low THz frequency bands are

The associate editor coordinating the review of this manuscript and approving it for publication was Vittorio Camarchia.

usually accomplished by using Schottky diodes. The multiplication/conversion efficiency provided by these solid-state devices represents the state-of-art, but it tends to drastically drop when considering multiplication orders greater than 2 or 3. To reach the submillimeter wave and low THz frequency bands from the microwave domain, the described problem is usually overcome by using topologies in which several low-order multiplier stages are interconnected in cascade [14], [15]. In consequence, the cost and complexity of the resulting topologies generally increase, due to the number of involved components and their required characteristics.

On the other hand, during the last few years, graphene has attracted great interest from the scientific community. Among its unique properties [16], the generation of an unlimited distribution of odd-order harmonic components with linearly decaying amplitude when a graphene sheet is exposed to an incident electromagnetic field was theoretically predicted [17], [18]. This capability was experimentally demonstrated through a wide variety of experiments covering from the low microwave region to the optical domain, describing the generation of second- [19]–[22] and third-order [23]–[25] harmonic components, and performing frequency mixing [26]–[28]. Furthermore, several graphene-based transistors [29]–[32] have also been reported.

The cited results were taken as the basis for the development of practical single-stage high-order frequency multipliers [7], [33]–[36] and sub-harmonic mixers [7], [37]–[40], covering the $140-500$ GHz frequency range, in which structured graphene sheets are used instead of Schottky diodes. The reported performance in terms of the output power, in the case of the frequency multipliers, or the mixing conversion efficiency, makes them suitable to be used in real applications [7], [36], [39], [40]. However, an accurate graphene simulation model was not available and, thus, they were designed following an iterative procedure.

In this work, we propose an approach to model the behavior of mono- and bi-layer graphene sheets in electromagnetic simulators, in order to calculate the level of the induced high-order harmonic components as a function of the exciting field strength, and to determine the frequency response of structures containing graphene. The described simulation strategy will be applied to the design and analysis of a single-stage high-order frequency multiplier based on a waveguide resonant cavity containing a graphene sheet, which generates an output signal in the $220-330$ GHz frequency range from an input signal in the $26-40$ GHz band. In addition, the performance of frequency multipliers using multi-layer graphene will be experimentally characterized. In this case, the developed model is used to calculate the frequency response of the structures, but it cannot be used to predict the output signal level, due to the lack of a mathematical model describing the harmonic generation in multi-layer graphene.

The work is organized as follows. Section II describes the topology of the proposed experiment and provides the guidelines of the modeling technique. In section III, implementation details are provided and experimental results obtained with mono- and bi-layer graphene are presented. Section IV is devoted to the analysis of several prototypes using multi-layer graphene, focusing on the optimization of the output power and their experimental characterization. Finally, the obtained results are analyzed in Section V.

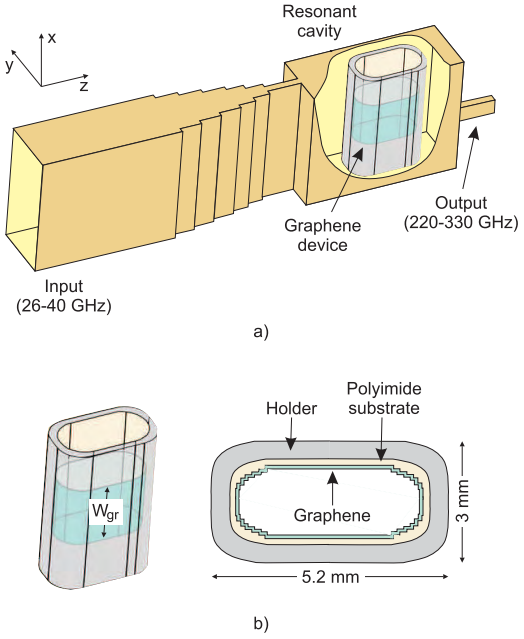

FIGURE 1. Topology of the experiment. (a) Waveguide block. (b) Detailed graphene device wrapped around the holder.

II. ANALYSIS OF MONO- AND BI-LAYER GRAPHENE DEVICES

A. TOPOLOGY OF THE EXPERIMENT

The experiment setup is schematized in Fig. 1 (a). It is composed of a rectangular resonant cavity which hosts the graphene device shown in Fig. 1 (b). It consists of a W_{gr} wide graphene strip deposited on a 25 μm thickness polyimide substrate with gold contacts at the ends. The relative dielectric permittivity and the loss tangent of the polyimide are $\varepsilon_r = 3.5$ and $\tan\delta = 0.008$, respectively. The obtained structure is rolled into a tube and the gold contacts are electrically connected using silver epoxy, in order to obtain a closed ring. That ring is introduced in a 300 μm thick holder implemented from acrylic resin, with $\varepsilon_r = 3.4$ and $\tan\delta = 0.008$. To excite the cavity with a signal at frequency f_{in} located in the $26-40$ GHz frequency range, it is connected to a standard WR28 rectangular waveguide through a tapered section which progressively reduces the input waveguide height. The output signal, with frequency $f_{out} = N \cdot f_{in}$, is generated due to the nonlinear response exhibited by the graphene layer driven by the input signal, and extracted from the cavity through a network composed of a standard WR3 rectangular waveguide section connected to the resonant cavity through a hole with the same cross section as the waveguide. Since the goal is to generate signal in the $220-330$ GHz range, $N = 7$ is considered.

First, the waveguide block is designed considering its performance in the input frequency band. The cross section of the cavity is identical to that of the standard WR28 in order to set the frequency of the first resonant mode TE_{101} in the $26-40$ GHz range. A length $l = 9.1$ mm, taken along $\hat{z}$ direction, was selected to excite the TE_{102} resonant mode at a frequency around 39 GHz, when it is empty. This mode was chosen because it provides two maximum values of the electromagnetic field along the cavity, with opposite phase. In this way, the graphene layer is simultaneously excited at two different points.

The tapered section of the input waveguide was optimized to maximize the cavity quality factor Q, and to minimize the return losses at the input port. Due to its dimensions, the effect of the output WR3 waveguide can be neglected when considering the system behavior in the $26-40$ GHz frequency band. The simulated input frequency response, when the cavity is empty, is represented with light grey trace in Fig. 2, showing that the resonance frequency of the fundamental mode is about 26 GHz, and that the TE_{102} mode occurs at 39 GHz. From the -3 dB bandwidth, the Q factor of the later is found to be around 1800.

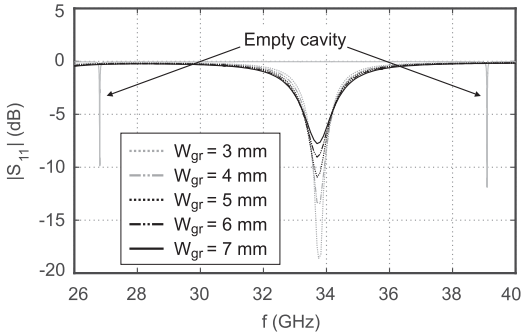

FIGURE 2. Comparison between the simulated frequency response of the empty and the filled cavity, as a function of the graphene strip width W_{gr}.

B. SIMULATION MODEL

Using the data provided by the graphene manufacturer, the mono-layer film is modeled as a 0.345 nm thickness sheet, with parallel conductivity $\sigma_{\parallel} = 6.44 \cdot 10^6$ S/m, and perpendicular conductivity $\sigma_{\perp} = 0$ S/m, whereas the bi-layer film presents a 0.69 nm thickness, $\sigma_{\parallel} = 5.79 \cdot 10^6$ S/m, and $\sigma_{\perp} = 0$ S/m. In order to overcome the limitations of the simulation software when assigning non-isotropic conductivity to a non-planar element, the curved regions of the graphene device were decomposed into planar sections, as represented in Fig. 1 (b).

The input frequency response of the system when the graphene device is placed in the cavity, as a function of the graphene strip width W_{gr}, is represented in Fig. 2. The strength of the resonant response increases when W_{gr} reduces, which means that the induced electric current reduces and, therefore, the cavity is less disturbed. A trade-off value $W_{gr} = 5$ mm was selected to provide an adequate resonant response while the induced current on the graphene sheet is high enough to excite the harmonic generation. Furthermore, due to the losses introduced by the graphene sheet, the quality factor is reduced to about 26, whereas the resonant frequency is shifted down because of the presence of the acrylic holder inside the cavity. The input frequency $f_{in} \approx 33.5$ GHz is selected to match the resonance frequency shown in Fig. 2, which corresponds to the TE_{102} mode of the filled cavity. The whole system was also analyzed using the eigenmode solver, revealing the existence of three additional resonances between 42.2 and 44.5 GHz, which are supposed to be caused by the interaction between the conductive graphene sheet and the cavity walls parallel to the XZ plane, and that are not revealed by the driven-mode simulation. Finally, when considering bi-layer graphene, similar performance is achieved reducing the strip width to $W_{gr} = 3$ mm.

C. ESTIMATION OF THE INDUCED HARMONIC COMPONENTS LEVEL

In order to calculate the output power in the $220-330$ GHz frequency band, the induced current density J_7 at the 7^{th} harmonic component of the input signal was calculate as:

$$J_7 = \frac{\sigma_7}{d} \cdot (E_{in})^7 \tag{1}$$

where d is the graphene layer thickness, E_{in} is the average value of the electric field tangential to the graphene sheet, and σ_7 is the 7^{th} order non-linear conductivity of the graphene, which has been calculated following the same procedure used in [17], [18]:

$$\sigma_7 = \frac{5^2 \cdot 3^2}{2^6} \cdot \frac{e^8 v_F}{\pi \hbar^7 (\pi n_s)^2 \sqrt{\pi n_s}} \cdot \frac{-7i}{\prod_{k=1}^{7} (k\omega + i/\tau)} \tag{2}$$

where $v_F = 10^6$ m/s is the Fermi velocity, n_s is the charge carrier density and τ is the electron relaxation time. The values $n_s = 0.875 \cdot 10^{16}$ m^{-2} and $\tau = 1.77^{-13}$ s have been derived for mono-layer graphene using the data provided by the graphene supplier, whereas $n_s = 1.56 \cdot 10^{16}$ m^{-2} and $\tau = 2.3^{-13}$ s were used in the case of bi-layer graphene. The computed values of the nonlinear conductivity are $\sigma_7 = 5.9 \cdot 10^{-35}$ and $\sigma_7 = 11 \cdot 10^{-35}$ S·m^6 · V^{-6} for the mono- and the bi-layer graphene, respectively.

Equation (1) is valid under the low field condition [17], [18]:

$$E_{in} << \frac{\omega \hbar \sqrt{\pi n_s}}{2e} \tag{3}$$

where $\hbar$ is the reduced Planck constant, and e is the electron electric charge. The computed value of E_{in}, as a function of the input signal power P_{in}, is represented in Fig. 3 (a), together with the limits calculated with (3). From the represented data, the induced current density J_7 at the 7^{th} harmonic of the input signal is obtained by applying (1). The obtained values are shown in Fig. 3 (b). It has been taken into account that (3) was theoretically derived assuming an ideal 2D-infinite isolated graphene sheet. Since these conditions

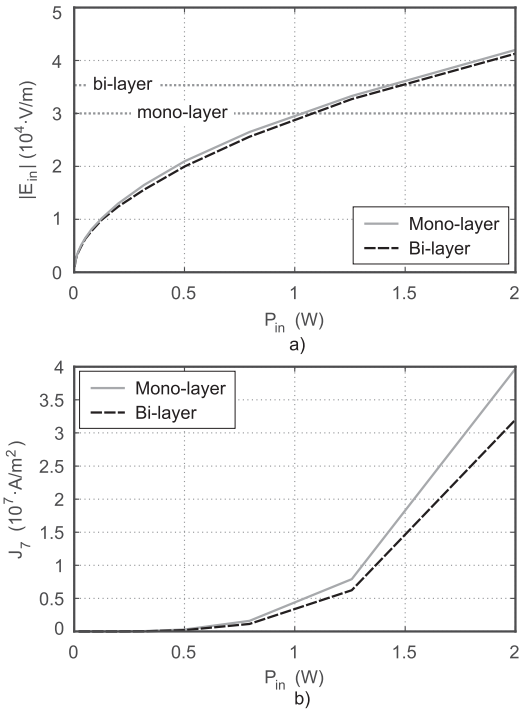

FIGURE 3. (a) Computed average electric field $|E_{in}|$ applied to the graphene sheet, as a function of the input signal power P_{in}, together with the low-field limit conditions. (b) Induced current density at the 7^{th} harmonic of the input signal, as a function of P_{in}.

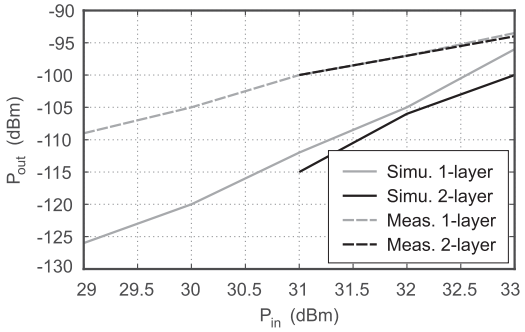

FIGURE 4. Predicted and measured values of the output signal power as a function of P_{in}.

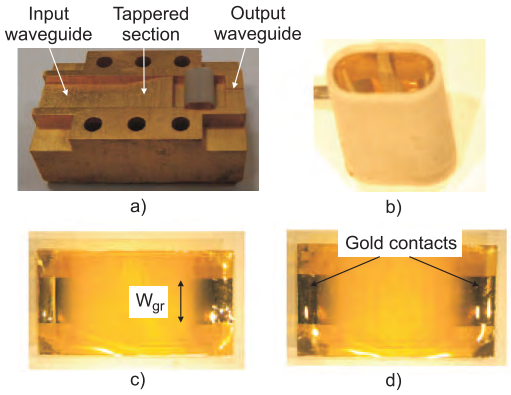

FIGURE 5. (a) Picture of one of the finished waveguide halves with the graphene holder placed in the cavity. (b) Detail of the graphene holder with the device wrapped inside. (c) Mono-layer graphene sample. (d) Bi-layer graphene sample.

cannot be met at any experimental device, deviations from the theoretical behavior are expected. At any case, works [17] and [18] represent the state-of-art about the electrodynamic behavior of grapehene.

Finally, the power of the output signal P_{out}, at frequency $f_{out} = N \cdot f_{in} = 239$ GHz, can be estimated by replacing the graphene layer with a current source working at frequency f_{out}, with nominal current value extracted from Fig. 3 (b). Once the induced current J_7 can be imposed in simulation, the associated field distribution can be calculated and the optimum connection point between the output waveguide and the cavity can be determined in order to maximize the output signal coupling. Furthermore, the point at which the input waveguide is connected to the resonant cavity can also be modified to minimize the portion of the output signal which is coupled back to the input port. The computed output signal power, evaluated at the output of the WR3 waveguide, is represented with dashed traces in Fig. 4. Because of the low-field limit, the accuracy of the results cannot be ensured for input power levels greater than 1 W.

III. EXPERIMENTAL RESULTS USING MONO- AND BI-LAYER GRAPHENE

A. IMPLEMENTATION DETAILS

A prototype was implemented to validate the described approach. The waveguide block was divided into two halves along the E-plane. They were implemented through a 3D stereo-lithography process using photo-sensible acrylic resin as base material, which was also used to manufacture the graphene device holder. Both parts of the waveguide block were covered with a gold layer with 1 μm estimated thickness by means of a sputtering process. The picture represented in Fig. 5 (a) shows one of the finished waveguide halves with the holder placed inside the resonant cavity.

The procedure followed to implement the graphene device involves several steps. First, a 25 μm thick polyimide sheet was cut to the desired shape. Next, 1 μm thick gold contacts were deposited along two opposite edges of the polyimide sheet. The mono- and bi-layer graphene films were first grown through CVD on copper substrate and then transferred to the polyimide and structured through a laser ablation process. Figures 5 (c) and (d) show pictures of the obtained graphene samples. Finally, the two gold contacts of each sample were joined together with silver based conductive glue, and the resulting structure placed inside the holder, as indicated in Fig. 5 (b).

B. EXPERIMENTAL RESULTS

The input frequency response of the implemented devices was measured using a conventional Vector Network Analyzer (VNA). It is represented in Fig. 6 together with simulation data. The measurement data reveals the resonances predicted

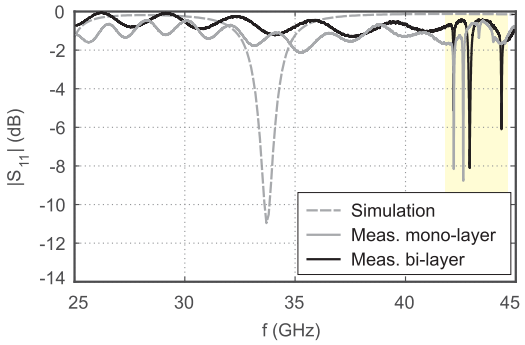

FIGURE 6. Measured input frequency response, together with simulation data.

using the eigenmode solver, but not the one derived from the analysis of the reflection coefficient in Fig. 2, which could be due to deviations between the implemented prototype and the simulated setup.

In order to measure the output power, the prototype was driven by an input signal provided by the VNA and amplified to reach the required input power P_{in}. Although the low field condition calculated with (3) establishes an input signal power threshold around 30 dBm, the minimum considered value is 29 dBm. This is due to the fact that it was experimentally found that lower power levels of the input signal provide an output signal with power under the noise floor of the measurement equipment, which is around -110 dBm. The output signal power was measured using a frequency extender module in combination with the VNA. The obtained results with the mono- and the bi-layer graphene devices are displayed in Figs. 7 (a) and (b), respectively, for different P_{in} values. Shaded areas relating the input and output frequency values were added to ease the data interpretation. Note that the output signal is only observable at frequency points $f_{out} = 7 \cdot f_{in}$, being f_{in} a point of the input frequency response for which the graphene is properly driven. Therefore, despite the unexpected measured input frequency response shown in Fig. 6, the experimental data represented in Fig. 7 is consistent with it, because the graphene is only excited at two (mono-layer) or three (bi-layer) f_{in} points around 42.5 GHz. On the one hand, the measured output power increases with P_{in}, whereas the frequency response reveals the existence of several resonant modes, which is in accordance with the measurement data shown in Fig. 6. On the other hand, the device presents a narrowband behavior. At this point, it has been taken into account that the graphene is theoretically expected to exhibit a flat nonlinear electromagnetic response from the microwave to the low-THz frequency range [17], [18]. Therefore, when used in practical applications, the obtained bandwidth is conditioned by the surrounding circuitry. In this particular case, the graphene sheet is excited by the input signal at narrowband input frequency regions, because of the input frequency response shown in Fig. 6.

The measured output peak power is compared with the theoretically predicted values in Fig. 4. First, the measured

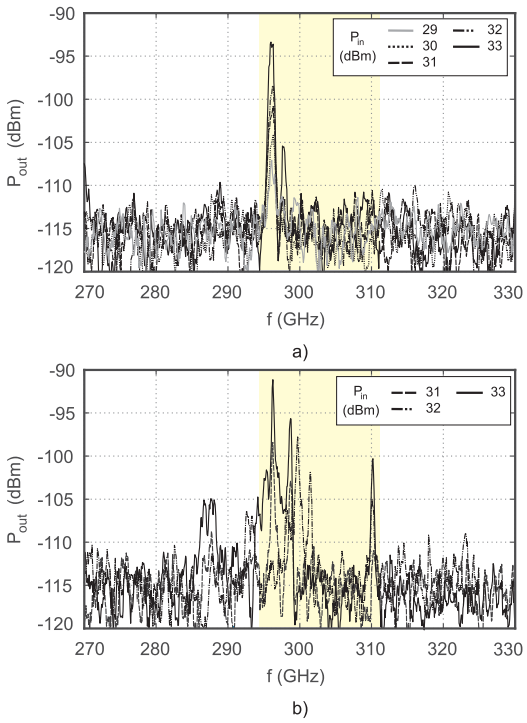

FIGURE 7. Evolution of the measured output power with P_{in}. (a) Mono-layer device. P_{in} varies from 29 to 33 dBm with 1 dB step. (b) Bi-layer device. P_{in} varies from 31 to 33 dBm with 1 dB step.

P_{out} values are considerably higher than those theoretically predicted. This is in accordance with the most recently published work about the nonlinear electrodynamic behavior of graphene [41], which predicts that the harmonic generation is significantly strengthened when the level of the incident electromagnetic field is higher than the limit imposed by (3). However, at this moment, these theoretical results cannot be used to develop a simulation model, since they have been obtained under certain particular assumptions, such working at $T = 0$ K, which are not reproducible when developing practical devices. Secondly, the measured output power values are nearly identical for the mono- and the bi-layer prototypes, which is in accordance with (1), considering that d and the computed σ_7 for the bi-layer case are approximately doubled with respect to the mono-layer case. Finally, the slope of the P_{out} *vs.* P_{in} characteristic is slightly lower than the theoretical value 7. This could be due to a saturation effect related to the low field condition expressed in (3), which establishes that the input power should be considerably lower than 1 W ($\equiv$ 30 dBm).

IV. EXPERIMENTAL RESULTS WITH MULTI-LAYER GRAPHENE

The measured output power levels using mono- and bi-layer graphene are too low to be exploited in practical applications. In this section, the design of several multi-layer graphene devices and their experimental characterization will be presented. The goal is to maximize the output power, considering

the three factors that are supposed to have the greatest influence, i. e., the level of the induced harmonic components on the graphene layers, the total device losses, and the coupling of the output signal to the WR3 waveguide.

A. MODELING AND IMPLEMENTATION DETAILS

The graphene devices employed in this case are similar to those previously presented, replacing the mono- or the bi-layer sheets with multi-layer films obtained through exfoliation from a Highly Ordered Pyrolytic Graphite (HOPG) block. Due to the lack of a model capable of accurately predicting the performance of multi-layer graphene in terms of harmonic generation, the simulator will only be used to calculate the input frequency response, in the 26−40 GHz range, whereas the output power will be experimentally determined. The multi-layer graphene sheet was modeled as a few-μm thickness layer with parallel and perpendicular conductivity values $\sigma_{\parallel} = 2.1 \cdot 10^6$, and $\sigma_{\perp} = 500$ S/m, respectively. Because of the unavailability of measurement equipment to accurately determine the number of graphene layers at our facilities, the sheet thickness was measured and its effect on the input frequency response was analyzed in simulation by varying it from 1 to 5 μm. From the obtained results, it was concluded that the layer thickness has little influence on the input frequency response. It is justified taking into account that the skin depth evaluated at 35 GHz is about $\delta \approx 1.8$ μm.

After exfoliating the HOPG and transferring the graphene sheets to the polyimide substrate, they were structured to obtain the desired shape. Regarding the waveguide block, the same structure that has been previously described was used.

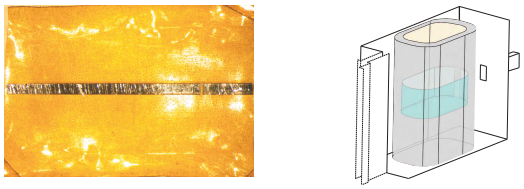

FIGURE 8. (a) Picture of the multi-layer graphene device employed in the prototype #1. (b) Assembly of the graphene device with the holder to be placed inside the cavity.

B. PROTOTYPE #1

The first tested device consists of a multi-layer graphene strip with a gap, as shown in Fig. 8 (a). The device is mounted in the holder and placed inside the cavity as schematized in Fig. 8 (b), joining together the two ends with silver-based conductive glue. The strip width W_{gr} and the gap width were optimized in order to achieve a strongly resonant response in simulation, obtaining the values $W_{gr} = 0.5$ mm and $W_{gap} = 50$ μm.

The simulated and measured input frequency responses are depicted in Fig. 9 (a). From the simulation data, the addition of the gap enhances the resonant response, and causes

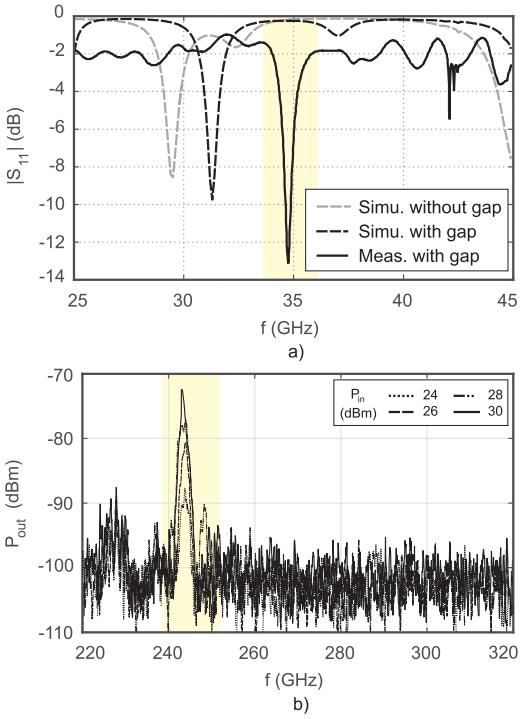

FIGURE 9. Experimental characterization of the prototype #1. (a) Input frequency response, compared with simulation data. (b) Evolution of the output power when P_{in} varies from 24 to 30 dBm, with 2 dB step.

the resonance to slightly shift towards higher frequencies. Furthermore, when comparing the measurement and the simulation data, an upward frequency shift is observed, providing a measured resonant frequency $f_{in} \approx 34.5$ GHz.

Regarding the performance as a frequency multiplier, the output power as a function of the input power P_{in} was measured, when varying it from 24 to 30 dBm with a 2 dB step. The obtained results are represented in Fig. 9 (b). As can be expected from the input frequency response, the power peak value is observed at frequency $f_{out} = 7 \cdot 34.5 = 241.5$ GHz, with a maximum output power $P_{out} = -72$ dBm.

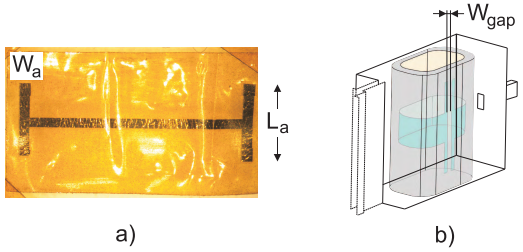

FIGURE 10. (a) Picture of the multi-layer graphene device employed in the prototype #2. (b) Assembly of the graphene device with the holder to be placed inside the cavity.

C. PROTOTYPE #2

Part (a) of Fig. 10 shows a picture of the graphene device, and part (b) schematizes its assembly on the holder to be inserted in the resonant cavity. The width of the strip is $W_{gr} = 0.5$ mm. In this case, two coupled lines, designed to resonate

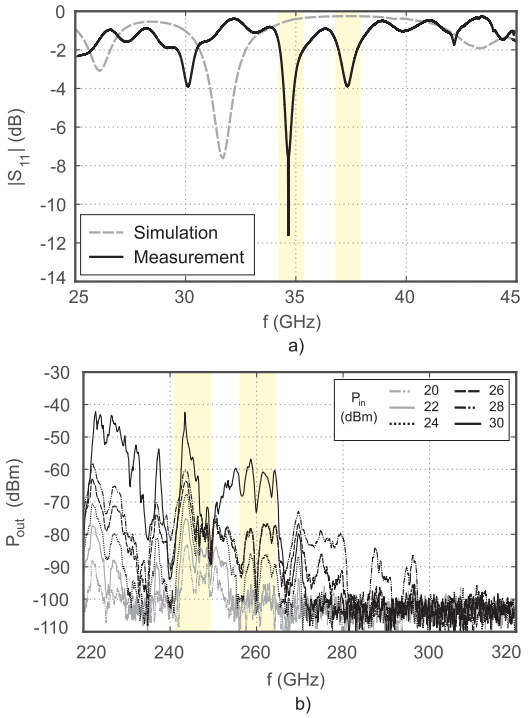

FIGURE 11. Experimental characterization of the prototype #2. (a) Input frequency response, compared with simulation data. (b) Output power. The input power varies from 20 to 30 dBm, with 2 dB step.

at about 30 GHz, were added. Their length and width are $L_a = 4.62$ mm, and $W_a = 0.3$ mm, respectively, and the gap between them when the structure is mounted on the holder is $W_{gap} = 0.3$ mm. In this case, the location of the coupled lines inside the cavity was selected to be in an area with low input field level.

The measured input frequency response is represented in Fig. 11 (a), together with simulation data, showing that the resonant frequency is around $f_{in} \approx 34.5$ GHz, and that the measured quality factor is higher than that predicted in simulation. On the other hand, the measured output power is shown in Fig. 11 (b), when the input power P_{in} varies from 20 to 30 dBm in 2 dB steps. The maximum reached value is around -44 dBm, and it is observed at frequency $f_{out} \approx 7 \cdot 34.5 = 241.5$ GHz. Furthermore, two additional regions with lower but appreciable power can be observed. They correspond to the 7^{th} harmonic component of input signals with frequency around 30.5 and 37 GHz, which are also able to excite the graphene device due to the input frequency response.

D. PROTOTYPE #3

The graphene device used in this case is represented in Fig. 12. Its shape is similar to that used in the prototype #2, but the length of the strip is reduced in half. The strip width $W_{gr} = 0.3$ mm was selected to maximize the strength of the resonant response. The device is placed inside the cavity as schematized in Fig. 12 (b), without using the holder.

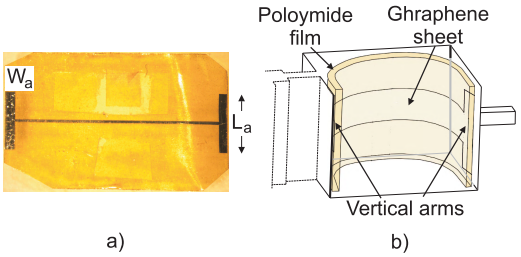

FIGURE 12. (a) Picture of the multi-layer graphene device employed in the prototype #3. (b) Assembly of the graphene device inside the cavity. Note that the holder is not used.

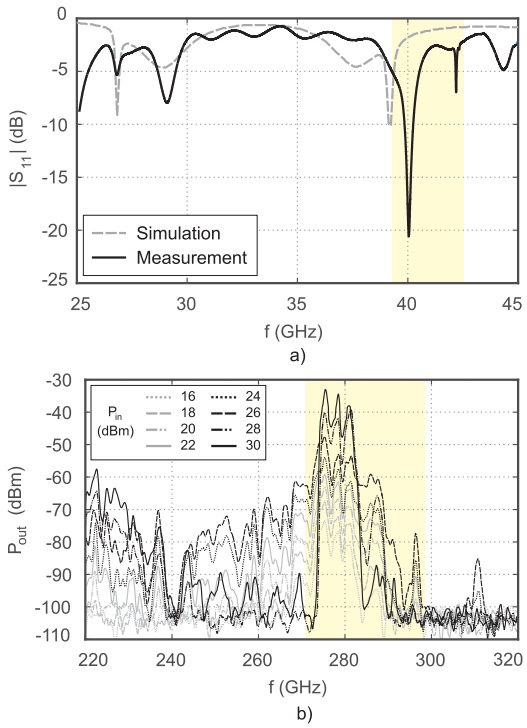

FIGURE 13. Experimental characterization of the prototype #3. (a) Input frequency response, compared with simulation data. (b) Output power. P_{in} varies from 16 to 30 dBm, with 2 dB step.

Figure 13 (a) represents the simulated and measured input frequency responses, showing the existence of two resonant modes at $f_{in} \approx 28$ and $f_{in} \approx 40$ GHz. The first one will not be considered in the analysis because the 7^{th} harmonic component of an input signal with that frequency would be located at $f_{out} = 196$ GHz, which is out of the nominal working range of the WR3 waveguides and the measurement devices. Since in this case the holder is not used, the simulated input frequency response is quite similar to that of the empty cavity shown in Fig. 2, with the expected reduction of the quality factor due to the losses of the graphene sheet. Furthermore, the resonant region around 42.5 GHz predicted using the eigen-mode solver is still observable because it is related with the local structures formed by the conductive graphene sheet and the cavity walls. On the other hand, in order to characterize the performance as frequency multiplier, the input power P_{in} was

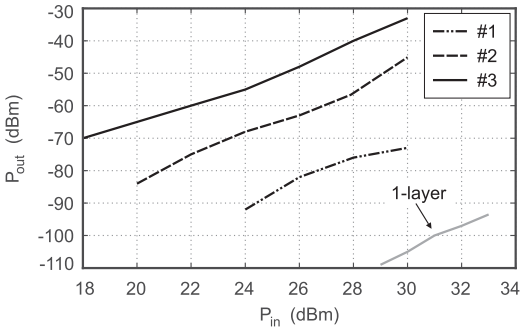

FIGURE 14. Evolution of the measured output power for the mono- and multi-layer prototypes. Note that, in each case, the output frequency is slightly different, depending on the particular input frequency response.

changed from 16 to 30 dBm, with a 2 dB step. The measured response is shown in Fig. 13 (b). The maximum response is observed at $f_{out} = 7 \cdot 40 = 280$ GHz, with a peak value $P_{out} = -33$ dBm.

V. DISCUSSION

From the comparison between the simulation and the experimental data represented in Figs. 9 (a), 11 (a), and 13 (a), the proposed multi-layer graphene simulation model exhibits a reasonably good performance, since it is able to predict the dominant resonances through driven-mode simulations, and the resonant region around 42.5 GHz using the eigenmode solver. Considering the prototypes #1 and #2, the most likely cause to explain the frequency shift of the dominant resonance is the use of an inaccurate value of the dielectric permittivity to model the holder structure. This is coherent with the fact that the deviation observed in the the prototype #3 is considerably lower, because the holder is not used. On the other hand, the resonant region around 42.5 GHz is observable in all the cases, even in the prototype #3, and does not suffer appreciable frequency deviation with respect to the simulated values. The reason is that such resonances are caused by the interaction between the graphene sheet and the cavity walls. Therefore, they mainly depend on the shape and the relative position of the graphene sheet, whereas a deviation on the relative permittivity of the holder material is expected to have a limited impact. Regarding the big deviation between the simulated and the measured input frequency response of the mono- and the bi-layer devices represented in Fig. 6, note that the only differences between the two devices and the multi-layer prototypes #1 and #2 are the shape and the number of layers of the graphene sheet, i. e., the total ohmic losses from the point of view of the input frequency response. Hence, the shape of the input frequency response and the position of the resonant points are expected to be very similar, as observed when comparing the simulation results presented in Figs. 6, 9 (a), and 11 (a). This fact supports the assumption that the absence of the fundamental resonance at $f_{in} \approx 34$ GHz in the measurements of the mono- and the bi-layer devices is due to an incorrect assembly. Figure 14 represents the maximum output power value reached by the tested mono- and multi-layer graphene devices, as a function of P_{in}. The output frequency in each case is slightly different, depending on the particular input frequency response of each prototype. Comparing the performance of prototype #1 with that of the mono-layer device, at $P_{in} = 30$ dBm, a 30 dB improvement is found. On the one hand, since the structure of the graphene device used in both cases is nearly identical, the performance improvement should be related to the increment in the number of graphene layers, which is aligned with the results presented in [23], [42]. In this case, we conclude that the output power increases with the number of layers of the graphene sheet due to the constructive combination of the signals induced at each individual one. This trend should saturate for a moderate number of layers (works [23], [42] estimate the limit to be around $n_{lim} = 20$) because the innermost layers are not directly excited by the input signal, since it is blocked by the outer layers. However, the results presented in [23], [42] were obtained in the optical domain. Here, when the number of layers and, thus, the cross section of the graphene device, is increased beyond n_{lim}, the ohmic losses are reduced and the available output power increases. Furthermore, since the slope of the traces at $P_{in} = 30$ dBm is still positive, the output power could be improved by increasing P_{in}. However, it was found that input power levels greater than 35 dBm cause the destruction of the graphene sheet by overheating. Therefore, $P_{in} = 30$ dBm was considered as a safety limit.

Secondly, the slope of all the traces associated to the multi-layer prototypes is below the expected 7 value, revealing that all the devices are saturated and the induced output signal is the maximum achievable for the considered P_{in} values. Note that the low field condition (3) is not applicable here, since it was derived for isolated ideal mono-layer graphene. Therefore, when comparing the multi-layer devices, it can be concluded that the output power variations are related to the coupling efficiency of the generated signal to the output waveguide, indicating that the performance of the presented devices could still be improved by optimizing the output signal coupling an by improving the thermal extraction capabilities of the devices.

TABLE 1. Performance comparison between the actual work and other recently published graphene-based frequency multipliers capable of generating signal at frequencies above 100 GHz.

Ref.	f_{out} (GHz)	P_{out} (dBm)	N	f_{in} (GHz)	P_{in} (dBm)
[33]	220-330	-30	7, 9, 11	26-40	21
[34]	330-500	-36	9-17	28-40	24
[35]	220-280	-50	7	31-40	0
[36]	220-330	-30	5, 7, 9	26-40	20
This work	280	-33	7	26-40	30

Table 1 summarizes a performance comparison between the presented device and other recently published graphene-based frequency multipliers capable of generating signal at

frequencies above 100 GHz. The maximum output power generated by the actual device $P_{out} \approx -33$ dBm is comparable to that of the other prototypes based on the same macroscopic graphene sheet technology. Therefore, although this value is far from the state-of-art represented by the Schottky diode technology, the proposed device could be used as signal generator in practical applications as the reported in [7] and [8]. The presented results demonstrates the technical viability of submillimeter wave graphene-based devices in short range applications, whereas the economic cost is dramatically reduced with respect to systems based on Schottky diodes.

VI. CONCLUSION

A simulation strategy to model the behavior of mono- and bilayer graphene sheets in electromagnetic simulators has been presented. The method is based on the currently available theoretical description of the graphene nonlinear electromagnetic response. It is able to predict the frequency response of structures using graphene, and to estimate the level of the induced high-order harmonic components. An experimental setup in which graphene layers were enclosed in a resonant cavity was designed to validate the proposed approach. The measured output power levels are considerably higher than those theoretically predicted, which is aligned with the most recently published works modeling the electrodynamics of graphene. The prototype was also used to experimentally characterize the behavior of multi-layer graphene, for which no mathematical model is still available. On the one hand, the variation of the output level with the input signal power reveals that the level of the induced harmonic components is the maximum achievable. On the other hand, the comparison between the mono- and the multi-layer devices performance shows that the output power can be increased using thicker graphene sheets to reduce the total losses. Finally, an output signal at 280 GHz with power around −33 dBm has been obtained, making the prototype usable in practical applications.

REFERENCES

[1] A. Luukanen, R. Appleby, M. Kemp, and N. Salmon, "Millimeter-wave and terahertz imaging in security applications," in *Terahertz Spectroscopy and Imaging* (Springer Series in Optical Sciences), vol. 171, Berlin, Germany: Springer, 2012, pp. 491–520.

[2] G. G. Hernandez-Cardoso, S. C. Rojas-Landeros, M. Alfaro-Gomez, A. I. Hernandez-Serrano, I. Salas-Gutierrez, E. Lemus-Bedolla, A. R. Castillo-Guzman, H. L. Lopez-Lemus, and E. Castro-Camus, "Terahertz imaging for early screening of diabetic foot syndrome: A proof of concept," *Sci. Rep.*, vol. 7, Jul. 2017, Art. no. 42124. doi: 10.1038/srep42124.

[3] F. Dornuf, P. Martín-Mateos, B. Duarte, B. Hils, O. E. Bonilla-Manrique, F. Larcher, P. Acedo, and V. Krozer, "Classification of skin phenotypes caused by diabetes mellitus using complex scattering parameters in the millimeter-wave frequency range," *Sci. Rep.*, vol. 7, Jul. 2017, Art. no. 5822. doi: 10.1038/s41598-017-06034-0.

[4] P. Martín-Mateos, F. Dornuf, B. Duarte, B. Hils, A. Moreno-Oyervides, O. E. Bonilla-Manrique, F. Larcher, V. Krozer, and P. Acedo, "*In-vivo*, non-invasive detection of hyperglycemic states in animal models using mm-wave spectroscopy," *Sci. Rep.*, vol. 6, Sep. 2016, Art. no. 34035. doi: 10.1038/srep34035.

[5] Z. D. Taylor, R. S. Singh, D. B. Bennett, P. Tewari, C. P. Kealey, N. Bajwa, M. O. Culjat, A. Stojadinovic, H. Lee, J.-P. Hubschman, E. R. Brown, and W. S. Grundfest, "THz medical imaging: *In vivo* hydration sensing," *IEEE Trans. THz Sci. Technol.*, vol. 1, no. 1, pp. 201–219, Sep. 2011. doi: 10.1109/TTHZ.2011.2159551.

[6] R. K. May, M. J. Evans, S. Zhong, C. Byers, L. F. Gladden, Y. Shen, and J. A. Zeitler, "Terahertz pulsed imaging of surface variations on pharmaceutical tablets," in *Proc. 35th Int. Conf. Infr., Millim., THz. Waves*, Rome, Italy, Sep. 2010, pp. 1–2. doi: 10.1109/ICIMW.2010.5612402.

[7] S. Ver Hoeye, M. Fernández, C. Vázquez, A. I. Hadarig, R. Camblor, L. Alonso, and F. Las-Heras, "Graphene based THz electromagnetic imaging system for the analysis of artworks," *IEEE Access*, vol. 6, pp. 66459–66467, 2018. doi: 10.1109/ACCESS.2018.2879161.

[8] C. Vázquez, R. Camblor, S. Ver Hoeye, A. I. Hadarig, G. Hotopan, M. Fernández, and F. Las-Heras, "Millimetre wave imaging system for the detection of hidden elements in artwork," in *Proc. Int. Conf. Electromagn. Adv. Appl.*, Palm Beach, Netherlands Antilles, Aug. 2014, pp. 675–678. doi: 10.1109/ICEAA.2014.6903943.

[9] I. Kemp, M. Peterson, C. Benton, and D. T. Petkie, "Sub-mm wave imaging techniques for non-destructive aerospace materials evaluation," in *Proc. IEEE Nat. Aerosp. Electron. Conf.*, Dayton, OH, USA, Jul. 2009, pp. 166–168. doi: 10.1109/NAECON.2009.5426634.

[10] E. Schlecht, G. Chattopadhyay, A. Maestrini, A. Fung, S. Martin, D. Pukala, J. Bruston, and I. Mehdi, "200, 400 and 800 GHz Schottky diode 'substrateless' multipliers: Design and results," in *IEEE MTT-S Int. Microw. Symp. Dig.*, Phoenix, AZ, USA, May 2001, pp. 1649–1652. doi: 10.1109/MWSYM.2001.967221.

[11] C. Lee, J. Ward, R. Lin, E. Schlecht, G. Chattopadhyay, J. Gill, B. Thomas, A. Maestrini, I. Mehdi, and P. Siegel, "A wafer-level diamond bonding process to improve power handling capability of submillimeter-wave Schottky diode frequency multipliers," in *IEEE MTT-S Int. Microw. Symp. Dig.*, Boston, MA, USA, Jun. 2009, pp. 957–960. doi: 10.1109/MWSYM.2009.5165857.

[12] D. Schneiderbanger, A. Cichy, R. Rehner, M. Sterns, S. Martius, and L.-P. Schmidt, "A hybrid broadband millimeter-wave diode ring mixer with advanced IF extraction technique," in *Proc. Eur. Microw. Conf.*, Munich, Germany, Oct. 2007, pp. 656–659. doi: 10.1109/EUMC.2007.4405277.

[13] P.-S. Wu, C.-S. Lin, T.-W. Huang, H. Wang, Y.-C. Wang, and C.-S. Wu, "A millimeter-wave ultra-compact broadband diode mixer using modified Marchand balun," in *Proc. Eur. Gallium Arsenide Semiconductor Appl. Symp.*, Paris, France, Oct. 2005, pp. 349–352.

[14] R. J. Dengler, F. Maiwald, and P. H. Siegel, "A compact 600 GHz electronically tunable vector measurement system for submillimeter wave imaging," in *IEEE MTT-S Int. Microw. Symp. Dig.*, San Francisco, CA, USA, Jun. 2006, pp. 1923–1926. doi: 10.1109/MWSYM.2006.249792.

[15] T. W. Crowe, J. L. Hesler, S. A. Retzloff, C. Pouzou, and G. S. Schoenthal, "Solid-state LO sources for greater than 2THz," in *22nd Space THz. Technol. Symp. Dig.*, Apr. 2011, pp. 1–4.

[16] M. M. Glazov and S. D. Ganichev, "High frequency electric field induced nonlinear effects in graphene," *Phys. Rep.*, vol. 535, no. 3, pp. 101–138, 2014. doi: 10.1016/j.physrep.2013.10.003.

[17] S. A. Mikhailov, "Non-linear electromagnetic response of graphene," *Europhys. Lett.*, vol. 79, no. 2, Jun. 2007, Art. no. 27002. doi: 10.1209/0295-5075/79/27002.

[18] S. A. Mikhailov and K. Ziegler, "Nonlinear electromagnetic response of graphene: Frequency multiplication and the self-consistent-field effects," *J. Phys., Condens. Matter*, vol. 20, no. 38, Aug. 2008, Art. no. 384204. doi: 10.1088/0953-8984/20/38/384204.

[19] M. Dragoman, A. Cismaru, A. Dinescu, D. Dragoman, G. Stavrinidis, and G. Konstantinidis, "Enhancement of higher harmonics in graphene-based coupled coplanar line microwave multipliers," *J. Appl. Phys.*, vol. 114, Oct. 2013, Art. no. 154304. doi: 10.1063/1.4825133.

[20] M. Dragoman, D. Neculoiu, G. Deligeorgis, G. Konstantinidis, D. Dragoman, A. Cismaru, A. A. Muller, and R. Plana, "Millimeter-wave generation via frequency multiplication in graphene," *Appl. Phys. Lett.*, vol. 97, Aug. 2010, Art. no. 093101. doi: 10.1063/1.3483872.

[21] J. J. Dean and H. M. van Driel, "Graphene and few-layer graphite probed by second-harmonic generation: Theory and experiment," *Phys. Rev. B, Condens. Matter*, vol. 82, Sep. 2010, Art. no. 125411. doi: 10.1103/PhysRevB.82.125411.

[22] A. Y. Bykov, T. V. Murzina, M. G. Rybin, and E. D. Obraztsova, "Second harmonic generation in multilayer graphene induced by direct electric current," *Phys. Rev. B, Condens. Matter*, vol. 85, no. 12, Mar. 2012, Art. no. 121413. doi: 10.1103/PhysRevB.85.121413.

[23] N. Kumar, J. Kumar, C. Gerstenkorn, R. Wang, H.-Y. Chiu, A. L. Smirl, and H. Zhao, "Third harmonic generation in graphene and few-layer graphite films," *Phys. Rev. B*, vol. 87, no. 12, Mar. 2013, Art. no. 121406. doi: 10.1103/PhysRevB.87.121406.

[24] S.-Y. Hong, J. I. Dadap, N. Petrone, P.-C. Yeh, J. Hone, and R. M. Osgood, Jr., "Optical third-harmonic generation in graphene," *Phys. Rev. X*, vol. 3, Jun. 2013, Art. no. 021014. doi: 10.1103/PhysRevX.3.021014.

[25] R. Camblor, S. Ver Hoeye, G. Hotopan, C. Vázquez, M. Fernández, F. Las-Heras, P. Álvarez, and R. Menéndez, "Microwave frequency tripler based on a microstrip gap with graphene," *J. Electromagn. Waves Appl.*, vol. 25, nos. 14–15, pp. 1921–1929, 2011. doi: 10.1163/156939311798072090.

[26] G. R. Hotopan, S. Ver Hoeye, C. Vazquez-Antuna, R. Camblor-Diaz, M. Fernandez-Garcia, F. L. H. Andres, P. Alvarez, and R. Menéndez, "Millimeter wave microstrip mixer based on graphene," *Prog. Electromagn. Res.*, vol. 118, pp. 57–69, Jun. 2011. doi: 10.2528/PIER11051709.

[27] G. R. Hotopan, S. Ver Hoeye, C. Vazquez-Antuna, A. I. Hadarig, R. Camblor-Diaz, M. Fernandez-Garcia, and F. L. H. Andres, "Millimeter wave subharmonic mixer implementation using graphene film coating," *Progr. Electromagn. Res.*, vol. 140, pp. 781–794, Jul. 2013. doi: 10.2528/PIER13042408.

[28] N. L. Rangel, A. Gimenez, A. Sinitskii, and J. M. Seminario, "Graphene signal mixer for sensing applications," *J. Phys. Chem. C*, vol. 115, pp. 12128–12134, Jun. 2011. doi: 10.1021/jp202790b.

[29] K. N. Parrish and D. Akinwande, "Even-odd symmetry and the conversion efficiency of ideal and practical graphene transistor frequency multipliers," *Appl. Phys. Lett.*, vol. 99, no. 22, 2011, Art. no. 223512. doi: 10.1063/1.3664112.

[30] M. E. Ramón, K. N. Parrish, S. F. Chowdhury, C. W. Magnuson, H. C. P. Movva, R. S. Ruoff, S. K. Banerjee, and D. Akinwande, "Three-gigahertz graphene frequency doubler on quartz operating beyond the transit frequency," *IEEE Trans. Nanotechnol.*, vol. 11, no. 5, pp. 877–883, Sep. 2012. doi: 10.1109/TNANO.2012.2203826.

[31] O. Habibpour, S. Cherednichenko, J. Vukusic, K. Yhland, and J. Stake, "A subharmonic graphene FET mixer," *IEEE Electron Device Lett.*, vol. 33, no. 1, pp. 71–73, Jan. 2012. doi: 10.1109/LED.2011.2170655.

[32] O. Habibpour, J. Vukusic, and J. Stake, "A 30-GHz integrated subharmonic mixer based on a multichannel graphene FET," *IEEE Trans. Microw. Theory Techn.*, vol. 61, no. 2, pp. 841–847, Feb. 2013. doi: 10.1109/TMTT.2012.2236434.

[33] S. Ver Hoeye, A. I. Hadarig, C. Vázquez, M. Fernández, L. Alonso, and F. Las-Heras, "Submillimeter wave high order frequency multiplier based on graphene," *IEEE Access*, vol. 7, pp. 26933–26940, 2019. doi: 10.1109/ACCESS.2019.2901577.

[34] A. I. Hadarig, C. Vázquez, M. Fernández, S. Ver Hoeye, G. R. Hotopan, R. Camblor, and F. Las-Heras, "Experimental analysis of the high-order harmonic components generation in few-layer graphene," *Appl. Phys. A, Solids Surf.*, vol. 118, pp. 83–89, Jan. 2015. doi: 10.1007/s00339-014-8739-y.

[35] A. I. Hadarig, S. Ver Hoeye, C. Vázquez, M. Fernández, G. Hotopan, R. Camblor, and F. Las-Heras, "7^{th} order sub-millimeter wave frequency multiplier based on graphene implemented using a microstrip transition between two rectangular waveguides," in *Proc. Int. Conf. Electromagn. Adv. Appl.*, Palm Beach, Netherlands Antilles, Aug. 2014, pp. 757–760. doi: 10.1109/ICEAA.2014.6903958.

[36] C. Vázquez, A. Hadarig, S. Ver Hoeye, R. Camblor, M. Fernández, G. Hotopan, L. Alonso, and F. Las-Heras, "Millimetre wave transmitter based on a few-layer graphene frequency multiplier," in *Proc. 45th Eur. Microw. Conf.*, Paris, France, Sep. 2015, pp. 510–513. doi: 10.1109/EuMC.2015.7345812.

[37] C. V. Antuña, A. I. Hadarig, S. Ver Hoeye, M. F. García, R. C. Díaz, G. R. Hotopan, and F. L. H. Andrés, "High-order subharmonic millimeter-wave mixer based on few-layer graphene," *IEEE Trans. Microw. Theory Techn.*, vol. 63, no. 4, pp. 1361–1369, Apr. 2015. doi: 10.1109/TMTT.2015.2403854.

[38] C. Vázquez, A. I. Hadarig, S. Ver Hoeye, M. Fernández, R. Camblor, G. Hotopan, and F. Las-Heras, "Millimetre wave subharmonic mixer based on graphene," in *Proc. Int. Telecommun. Symp.*, Sao Paulo, Brazil, Aug. 2014, pp. 1–5. doi: 10.1109/ITS.2014.6948016.

[39] C. Vázquez, A. Hadarig, S. Ver Hoeye, R. Camblor, M. Fernández, G. Hotopan, L. Alonso, and F. Las-Heras, "Millimetre wave receiver based on a few-layer graphene WR-5 band subharmonic mixer," in *Proc. Global Symp. Millim.-Waves*, Montreal, QC, Canada, May 2015, pp. 1–3. doi: 10.1109/GSMM.2015.7175433.

[40] A. I. Hadarig, S. Ver Hoeye, C. Vázquez, R. Camblor, M. Fernández, G. Hotopan, L. Alonso, and F. Las-Heras, "3D printed millimeter wave receiver integrating a graphene subharmonic mixer and a diagonal horn antenna," in *Proc. Global Symp. Millim.-Waves*, Montreal, QC, Canada, May 2015, pp. 1–3. doi: 10.1109/GSMM.2015.7175434.

[41] S. A. Mikhailov, "Nonperturbative quasiclassical theory of the nonlinear electrodynamic response of graphene," *Phys. Rev. B, Condens. Matter*, vol. 95, Feb. 2017, Art. no. 085432. doi: 10.1103/PhysRevB.95.085432.

[42] E. Hendry, P. J. Hale, J. Moger, A. K. Savchenko, and S. A. Mikhailov, "Coherent nonlinear optical response of graphene," *Phys. Rev. Lett.*, vol. 105, Aug. 2010, Art. no. 097401. doi: 10.1103/PhysRevLett.105.097401.

ANDREEA IOANNA HADARIG received the B.Sc. degree in telecommunication engineering from the Technical University of Cluj-Napoca, Romania, in 2012, and the M.Sc. degree in information technology and mobile communications and the Ph.D. degree from the University of Oviedo, Spain, in 2013 and 2017, respectively.

Since 2012, she has been a Research Assistant with the Signal Theory and Communications Group, University of Oviedo. Her main research interests include the design, optimization, and analysis of passive devices using waveguides and microstrip technology operating in the millimeter-/submillimeter-wave and THz frequency bands.

SAMUEL VER HOEYE (M'05) received the M.Sc. degree in electronics engineering from Ghent University, Ghent, Belgium, in 1999, and the Ph.D. degree from the University of Cantabria, Santander, Spain, in 2002.

He is currently an Associate Professor with the Department of Electrical and Electronic Engineering, University of Oviedo, Gijón, Spain. His main research interests include the design and analysis of microwave, millimeter-wave, and THz circuits and systems, including the multi-functional oscillator-based circuits and antennas, frequency scanning antennas, graphene-based frequency multipliers and mixers, imaging systems, and textile-integrated high-frequency components.

MIGUEL FERNÁNDEZ received the M.Sc. degree in telecommunication engineering, the M.Sc. degree in information technology and mobile communications, and the Ph.D. degree from the University of Oviedo, Gijón, Spain, in 2006, 2010, and 2010, respectively.

From 2006 to 2008, he was a Research Fellow with the Signal Theory and Communications Group, University of Oviedo, where he has been an Associate Professor, since 2008. His main research interests include nonlinear analysis and optimization techniques for the design of oscillator-based circuits, active antennas, and frequency multipliers and mixers at the microwave, millimeter-/submillimeter-wave, and terahertz frequency bands.

SERGEY MIKHAILOV received the Diploma degree in physics from the Moscow Institute of Physics and Technology, in 1982, the Ph.D. degree in physical and mathematical sciences from the Institute of Radioengineering and Electronics, Russian Academy of Sciences, in 1987, and the Habilitation degree in theoretical physics from the University of Augsburg, Germany, in 2013. He worked at different universities and research institutes in Russia, Germany, Sweden, and Japan. Since 2006, he has been with the Department of Physics, University of Augsburg, where he studies linear and nonlinear electrodynamic and optical properties of graphene. He has edited two books and authored several patents, about 100 papers in journals and book collections, and more than 100 conference presentations. His current research interests include the theory of low-dimensional electron systems in semiconductor heterostructures, graphene, and graphene-related materials. He was a Fellow of the Alexander von Humboldt Foundation, Germany, in 1995, and a Senior Fellow of the Japan Society for the Promotion of Science, in 2005. He was a Principal Investigator of several research projects funded by National and European research agencies.

CARLOS VÁZQUEZ received the M.Sc. degree in telecommunication engineering, the M.Sc. degree in information technology and mobile communications, and the Ph.D. degree from the University of Oviedo, Gijón, Spain, in 2007, 2008, and 2013, respectively.

From 2007 to 2012, he was a Graduate Research Assistant with the Signal Theory and Communications Group, University of Oviedo, where he has been a Research Fellow, since 2012. His research interests include nonlinear analysis and optimization techniques for the design of multifunctional oscillator-based circuits, active antennas, and passive components, such as frequency multipliers and harmonic mixers, at microwave, millimeter-/submillimeter-wave, and terahertz frequencies.

LETICIA ALONSO received the M.Sc. degree in telecommunication engineering from the University of Oviedo, Gijón, Spain, in 2014, the M.Sc. degree in systems and control engineering from the National University of Distance Learning (UNED) and the Universidad Complutense de Madrid, Spain, in 2018, and the Ph.D. degree from the University of Oviedo, in 2018.

Since 2014, she has been a Researcher with the Signal Theory and Communications Group, University of Oviedo. She was a Visiting Scholar with the George Green Institute for Electromagnetics Research, University of Nottingham, U.K., in 2017. Her main research interests include the design, simulation, and manufacturing techniques to develop microwave- and millimeter-wave passive circuits and antennas fully integrated in textile technology.

FERNANDO LAS-HERAS received the M.S. and Ph.D. degrees in telecommunication engineering from the Technical University of Madrid (UPM), in 1987 and 1990, respectively. He was the National Graduate Research Fellow and an Associate Professor with the Department of Signal, Systems, and Radiocom, UPM, from 1988 to 1990 and from 1991 to 2000, respectively. Since 2001, he has been the Head of Research Group Signal Theory and Communication (TSC-UNIOVI), Department of Electrical Engineering, University of Oviedo. Since 2003, he has been a Full Professor with the University of Oviedo. He was the Vice-Dean for Telecommunication Engineering with the Tech School of Engineering, Gijón, from 2004 to 2008. He was a Visiting Researcher with Syracuse University, New York, and a Visiting Lecturer with the National University of Engineering, Lima, and ESIGELEC, France. He has authored over 450 technical journals and conference papers in the areas of electromagnetic radiation, propagation and scattering theory and applications as well as inverse problems. He was a member of the Science, Technology, and Innovation Council of Asturias, Spain, in 2010, the Board of Directors of the IEEE Spain Section, from 2012 to 2015, and the Board of the IEEE Microwaves & Antennas Propagation Chapter (AP03/MTT17), from 2016 to 2018. He held the Telefónica Chair on RF technologies, ICTs applied to environment and climate change, and ICTs and smartcities, from 2005 to 2015.